Accepted Manuscript

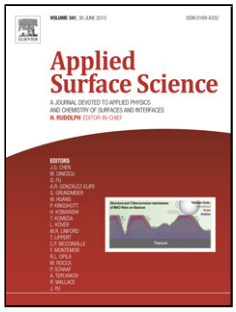

Title: A DFT study of phenol adsorption on a low doping Mn–Ce composite oxide model

Author: Oriana DĭAlessandro Delfina García Pintos Alfredo Juan Beatriz Irigoyen Jorge Sambeth

PII: S0169-4332(15)02397-1
DOI: http://dx.doi.org/doi:10.1016/j.apsusc.2015.09.266
Reference: APSUSC 31480

To appear in: *APSUSC*

Received date: 7-9-2015
Revised date: 29-9-2015
Accepted date: 30-9-2015

Please cite this article as: O. DĭAlessandro, D.G. Pintos, A. Juan, B. Irigoyen, J. Sambeth, A DFT study of phenol adsorption on a low doping MnndashCe composite oxide model , *Applied Surface Science* (2015), http://dx.doi.org/10.1016/j.apsusc.2015.09.266

Ms. Ref. No.: APSUSC-D-15-06577 revision # 1

A DFT study of phenol adsorption on a low doping Mn–Ce composite oxide model

Oriana D´Alessandro[1], Delfina García Pintos[2], Alfredo Juan[3*], Beatriz Irigoyen[2], Jorge Sambeth[1]

[1] CINDECA – Fac. Cs. Ex. UNLP, CCT – CONICET, Calle 47 Nro. 257, (1900) La Plata, Argentina.

[2] ITHES–UBA, Pabellón de Industrias, (1428) Buenos Aires, Argentina.

[3] Departamento de Física & IFISUR – UNS, Avda. Alem 1253, (8000) Bahía Blanca, Argentina.

** E–mail: cajuan@uns.edu.ar*

Tel. Number: +54 2914595142

Abstract

Density functional theory calculations (DFT+U) were performed on a low doping Mn–Ce composite oxide prepared from experimental data, including X-ray diffraction (XRD) and temperature-programmed reduction (TPR). We considered a 12.5% Mn–doped CeO_2 solid solution with fluorite–type structure, where Mn replaces Ce^{4+} leading to an oxygen–deficient bulk structure. Then, we modeled the adsorption of phenol on the bare $Ce_{0.875}Mn_{0.125}O_{1.9375}$(111) surface. We also studied the effect of water adsorption and dissociation on phenol adsorption on this surface, and compared the predictions of DFT+U calculations with diffuse reflectance infrared Fourier transform spectroscopy (DRIFTS) measurements. The experimental results allowed us to both build a realistic model of the low doping Mn–Ce composite oxide and support the prediction that phenol is adsorbed as a phenoxy group with a tilt angle of about 70° with respect to the surface.

Keywords: Phenol Adsorption, DRIFTS, Phenoxy, DFT, CeO_2

1. Introduction

Cerium oxide based materials with promoted structural and electronic properties have attracted attention due to their technological applications as both mass catalysts and supports of metal active phases [1–4]. Generally, these materials present a considerable number of surface and bulk oxygen defects, which results in improved oxygen storage capacity (OSC). The capacity to accept or to release oxygen is mainly related to cerium ability to form Ce^{4+}/Ce^{3+} couples [5,6]. The performance of cerium oxide can be improved with the addition of late transition, alkaline or rare earth metals [1,7]. Particularly, the incorporation of transition metals facilitates the formation of oxygen vacancies, leading to CeO_2–based materials with enhanced OSC and improved redox properties [7–10]. Doping or incorporation of Mn into the fluorite–type structure of CeO_2 results in catalysts with remarkable activity in oxidation processes. Accordingly, CeO_2–MnO_x solid solutions have shown excellent OSC and catalytic performance in many valuable processes, such as oxidation of diesel soot, ethanol, formaldehyde and phenol, selective reduction of NO with NH_3, and oxidation of small hydrocarbon molecules and CO [11–19].

Liquid effluents from petrochemical, carbochemical, pharmaceutical, paper and painting industries contain toxic chemical substances such as phenol and must be treated before discharging. Phenol is a very harmful substance not only to aquatic organisms but also to human beings, even when it is present in small concentrations. The high stability of this molecule makes degradation with traditional water purification methods very difficult. Two methods have been evaluated by different authors, the destructive and the recovery processes, with the purpose of reducing phenol concentration in wastewater. The adsorption of phenol is considered as a recovery process, and various adsorbents are used for phenol removal such as activated carbon, silica gel, iron oxide, polymeric resins, and fly ash. Phenol is also an intermediate product in the oxidation of higher–molecular–weight aromatic compounds [20]. Thus, several authors have studied the adsorption of organic compounds from aqueous solution onto manganese oxide, and their results have shown that the adsorption process is a function of the morphology, the presence of other cations, and the oxidation states of Mn [21–24]. In this regard, low cost MnO_x–based catalysts instead of noble metal catalysts have been investigated in the catalytic wet oxidation (CWO) of phenolic wastewater [25–27]. Arena et al. [28] have proposed that the catalytic destruction of phenol occurs in a five–step adsorption–oxidation process: (i) adsorption on the surface, (ii) substrate/sorbent interaction, (iii) phenolic intermediate species formation, (iv) CO_x formation, and (v) surface reoxidation. More recently, D´Alessandro et al. [24] have analyzed the species formed in the first step of the

phenol adsorption–oxidation on the $MnCeO_x$ surface by DRIFT spectroscopy and demonstrated that phenol is adsorbed as phenolate species at the initial step. However, the first stage of phenol adsorption on the CeO_2–MnO_x surface, which plays an important role in electron transfer and oxygen reduction, has not yet been fully understood.

There are several density functional studies of phenol adsorption on transition metals, nanotubes, BN sheets, carbon-based materials and semiconductors. On the other hand, theoretical studies of phenol adsorption on transition metal oxides are rather scarce. The structure and energetics of phenol in vertical ring geometry on Ni (111), (110), and (221) surfaces was studied by Site et al. and Ghiringhelli et al. [29,30]. These last authors considered the possible oxygen–surface bond and O–H cleavage. Altarawneh et al. [31,32] performed first principles calculations for chlorophenol on Cu(1 0 0) and Cu(111); the molecule is very weakly bound to the Cu(1 0 0) surface. Jayanthi et al. [33] performed DFT studies on the phenol and thiophenol interaction on an undecagold cluster surface and found that the O–H or S–H bonds were activated on the Au surface. Hensley et al. [34, 35] studied the adsorption of phenol on Fe (110) and Pd (111) surfaces with van der Waals corrections. They reported that phenol adsorption via the aromatic ring (parallel) is significantly more favorable than via the oxygen functional group (perpendicular). In the case of Pt(111) and Pd(111), Li et al. [36] simulated the adsorption, dissociation, and hydrogenation of phenol. Their results show that phenol favors adsorption through a mixed σ–π interaction on both surfaces through its phenyl ring, with the hydrogen atoms and hydroxyl tilted away from the surface. Zhao et al. [37] studied phenol adsorption on a semiconducting (8, 0) silicon carbide nanotube and found that the hydroxyl group prefers to attach to a Si atom. The calculated adsorption energy is –0.494 eV and 0.208e are transferred from the adsorbate to the nanotube, while the O–H bond can be split on the nanotube. DFT calculations for the adsorption of phenol on Ga- and In-doped armchair boron nitride nanotubes indicate that the hydroxyl group can lead to significant interactions on the surface, with binding energies on Ga and In sites of –1.18 and –0.93eV, respectively [38,39]. In the case of Ga and Pd on (6, 0) zigzag boron phosphide nanotubes, the adsorption energies were –0.724 and –0.420 eV, respectively [38,39]. Phenol is chemisorbed on nanocages with energies on Al12N12 and Al12P12 of −1.03 and −0.76 eV, respectively [40]. Galicia Hernández et al. [41,42] considered phenol adsorption on boron nitride sheets and Al–doped graphene. These authors predict a configuration where the O and Al atoms interact with a separation distance of 1.97 Å. DFT calculations were utilized to investigate the adsorption of phenol-activated carbon [43]. The molecule undergoes weak physical adsorption due

to van der Waals interactions between the aromatic part of phenol and the basal planes. The transition in the molecular orientation of phenol adsorbates on the Ge(100) and Si (100) – 2 × 1 surfaces were studied by Shong and Bent, and Carbone et al. [44–46]. Both groups found that phenol chemisorbs via O–H dissociation to form adsorbed phenoxy. First principles calculations of phenol adsorbed on α–Al_2O_3(0001) were performed by Chakarova–Käck et al. and Blomqvist and Salo [47,48]. These authors reported a binding separation between surface Al and the O of the inclining phenol molecule of 1.95 Å and an energy of 1.2 eV. Altarawneh et al. [49] explored the adsorption of a two–chlorophenol molecule on Cu_2O(110) and found very weakly interactions forming several vertical and flat orientations. These weakly bound states tend to result from the interaction between the phenolic hydrogen and an oxygen surface atom.

Despite the extensive theoretical research previously described, to the best of our knowledge there are no DFT calculations of phenol adsorption on CeO_2–MnO_x solid solutions. In fact, only few researchers have performed fundamental studies on these materials. Tang et al. [50] investigated the redox thermodynamics of doped CeO_2 bulk structure with 3.125 and 6.25 % Mn, Pr, Sn, or Zr, obtaining the lowest O–vacancy formation energy for the Mn–doped system. Gupta et al. [51] studied the distortions introduced in the bulk structure of CeO_2 when combined with different metals M (M: Mn, Fe, Co, Ni, Cu), concluding that the longer the M–O bond lengths, the higher the M–Ce mixed oxide OSC. Cen et al. [52] evaluated the reduction and reoxidation processes of a CeO_2(111) slab in which one of the surface Ce atoms was replaced by Mn. A similar model was employed by Zhang et al. [53], who reported not only theoretical but also experimental results showing that a Mn–doped CeO_2 solid solution has a higher oxygen storage capacity than pure CeO_2.

Therefore, the objective of the present investigation is first to build a realistic model of Mn–doped CeO_2 solid solutions based on experimental data, and second to study, at theoretical level, phenol adsorption and the influence of hydroxyls on that aromatic compound interaction on the solid surface. We will also compare the theoretical predictions about phenol adsorption and water dissociation influence on its adsorption mechanism, with DRIFTS studies.

2. The Mn–doped Ce oxide surface model

Starting from X–ray diffraction (XRD) and temperature-programmed reduction (TPR) data, we developed a model for a partially reduced Ce oxide surface. The XRD

spectrum of Mn–Ce oxide with molar ratio 10–90 was recorded using samples prepared by coprecipitation of $Ce(NO_3)_3 \cdot 6H_2O$ (Sigma–Aldrich) and $Mn(NO_3)_2 \cdot 4H_2O$ (Anedra) at pH = 11, following the method of Imamura et al. [54]. This spectrum (see Fig. 1) only shows the presence of CeO_2 (fluorite–type structure JCPDS # 43–1002, with a lattice parameter value of 5.4113 Å). The absence of diffraction peaks corresponding to MnO_x allows us to consider that Mn cations enter the CeO_2 fluorite structure, leading to the formation of Mn–Ce oxide solid solution. The results showed the formation of a solid solution where Mn replaces tetravalent Ce cations. The partial replacement of Ce^{4+} by Mn is probable, knowing that the incorporation of Mn^{2+} or Mn^{3+} into the lattice decreases the lattice parameter as the ionic radii of Mn^{2+} (0.066 nm), Mn^{3+} (0.062 nm) and Mn^{4+} (0.053 nm) are smaller than that of Ce^{4+} (0.097 nm).

We decided to choose a unit cell formula of $Ce_{0.875}Mn_{0.125}O_2$ (12.5% Mn–doped CeO_2) that is close to the experimental composition ($Ce_{0.90}Mn_{0.10}O_x$) while keeping the size suitable for computational purposes. According to this, the supercell consists of 2 x 2 x 2 CeO_2 unit cells formed by 28 Ce cations, 4 Mn cations and 64 oxygen anions, and we calculated its optimized lattice constant value as 5.463 Å [55]. A schematic view of the crystal lattice with oxygen vacancies is shown in Fig. 2.

Figure 1

Figure 2

Figure 3 shows the H_2–TPR profiles of MnOx and $Ce_{0.90}Mn_{0.10}O_x$. TPR of MnOx shows two maxima at ca. 340 ºC and 460 ºC, which are associated with the $MnO_2/Mn_2O_3 \rightarrow Mn_3O_4$ and $Mn_3O_4 \rightarrow MnO$ processes, respectively [56,57]. The reduction of Mn is promoted by the formation of the solid solution. As can be seen, the reduction peaks are shifted at lower temperatures with two maxima at ca. 300 ºC and 400 ºC. Additionally, in the $Ce_{0.90}Mn_{0.10}O_x$ sample, a broad peak is observed at ca. 260 ºC. On the basis of results reported by Kapteijn et al. [58], this broad peak may be attributed to the reduction of highly dispersed MnO_x species. According to Qi et al. [59] and our results, we can conclude that oxygen mobility in the solid solution is improved by Mn–Ce interaction. The decrease in the reduction temperature demonstrates that reductions of Mn and Ce oxides are promoted by Mn–Ce interaction. This interaction is favored by the formation of a solid solution in which the mobility of oxygen species is enhanced.

Figure 3

The removal of two O anions from the bulk supercell model represents this reduction process and leads to a more stable O–deficient structure with $Ce_{0.875}Mn_{0.125}O_{1.9375}$ composition. The catalyst surface model was obtained by cutting the structural–oxygen–deficient bulk structure with the (111) plane (as indicated in Fig. 2). Thus, for the study of phenol interactions on the 12.5% Mn–doped CeO_2 catalyst, we employed the same $Ce_{0.875}Mn_{0.125}O_{1.9375}$(111) surface model as in previous work [55,60], a stack of O–cations–O sandwiches terminated with an extra O–layer (see Fig. 4a). Then, this surface was modeled with a slab formed by twelve atomic layers, two structural oxygen vacancies and a vacuum space of 20 Å in order to avoid periodic interactions with the atoms of the upper image. The Brillouin zone was sampled with a 3 x 2 x 1 k-points grid, according to the Monkhorst-Pack scheme. For all energy calculations we allowed phenol and Ce, Mn and O ions located in the six uppermost layers of the slab to fully relax, while keeping the atomic positions of the ions fixed at the six lowermost layers.

Figure 4 (a and b)

The structural–oxygen–deficient $Ce_{0.875}Mn_{0.125}O_{1.9375}$(111) slab exposes Ce cations with different environments and Mn cations also. In Fig. 4b, we labeled the surface cations that were considered for studying phenol interactions as Ce2, Ce5, Ce6, Ce7 and Mn1. Note that Ce1 is equivalent to Ce5, Ce2 to Ce4, and Ce3 to Ce7. In addition, Ce2 and Ce4 are located near a structural O–vacancy, Ce1 and Ce5 are close to the Mn dopant, and Ce3 and Ce6 are neighbored by Mn1 and a structural O–vacancy.

3. Theoretical method and calculation details

In this work, we performed density functional theory (DFT) calculations using the Vienna Ab–initio Simulation Package (VASP) [61,62]. In this respect, Kohn–Sham equations were solved with the generalized gradient approximation (GGA) and the exchange–correlation functional of Perdew–Burke–Ernzerhof (PBE) [63]. The core electrons were represented by the projector augmented wave (PAW) method [64]. The valence electron wave functions were expanded using a truncation energy value of 408 eV. For valence configurations we used Ce($5s^2$, $5p^6$, $6s^2$, $5d^1$, $4f^1$), Mn($3d^6$, $4s^1$), O($2s^2$, $2p^4$), C($2s^2$, $2p^2$) and H($1s^1$). The Brillouin zone was sampled with a 3 x 2 x 1 k–point grid according to the Monkhorst–Pack scheme [65]. The structural relaxations were

performed according to the Hellmann–Feynman approximation, and the atomic positions were relaxed until the force acting on each atom was smaller than 0.02 eV/Å. For all energy calculations we considered the spin polarization effects.

The standard DFT formulation usually fails to describe strongly correlated electrons. This limitation was corrected by using the DFT+U method, where the introduction of a Hubbard parameter U modified the self–interaction error and enhanced the description of the correlation effects [66,67]. According to our previous study [55], we used Hubbard parameters: U = 5 eV for Ce(4f) states, and U = 4.5 eV for Mn(3d) orbitals.

The phenol adsorption energy was calculated as:

$$\Delta E_{ads,phenol} = E[Phenol/Ce_{0.875}Mn_{0.125}O_{1.9375}(111)] - E[Ce_{0.875}Mn_{0.125}O_{1.9375}(111)] - E[Phenol],$$

where $E[Phenol/Ce_{0.875}Mn_{0.125}O_{1.9375}(111)]$ represents the total energy of the system resulting from the molecular adsorption of phenol on the structural–oxygen–deficient $Ce_{0.875}Mn_{0.125}O_{1.9375}(111)$ surface. $E[Ce_{0.875}Mn_{0.125}O_{1.9375}(111)]$ is the total energy of the structural–oxygen–deficient bare surface, while E[Phenol] represents the energy of a phenol molecule in vacuum. A negative value of $\Delta E_{ads,phenol}$ indicates stabilization of the adsorbate and a favorable process.

4. Results and Discussion

We report the computed molecular interactions of phenol on both the clean and the hydroxylated $Ce_{0.875}Mn_{0.125}O_{1.9375}(111)$ surfaces. Thus, different surface active sites were considered in the present study: O anions, Ce and Mn cations, and OH groups also.

Concerning the hydroxylated $Ce_{0.875}Mn_{0.125}O_{1.9375}(111)$ surface, previous DFT+U calculations have indicated that molecular and dissociated interactions of water involve a surface Mn–dopant cation [60]. Table 1 lists the computed energy values for both the molecular and the dissociated interactions of H_2O on different surface Ce and Mn cations of the structural–oxygen–deficient $Ce_{0.875}Mn_{0.125}O_{1.9375}(111)$ surface [55]. The preferred adsorption of H_2O molecule on a Mn cation ($\Delta E_{ads,H2O}$ = –0.81 eV) causes some relaxation of the surface O–layer and, thus, facilitates the bonding of one of the H_{water} with the nearest surface oxygen anion. Moreover, the most exothermic water dissociated interactions led to bonding of the OH fragment to a Mn cation and that of

the H species to an O_{Ce} anion (see Fig. 5). The computed energy value ($\Delta E_{ads,OH-H}$ = –1.21 eV) implies that water underwent strong dissociative chemisorption on Mn dopant at the $Ce_{0.875}Mn_{0.125}O_{1.9375}(111)$ surface. In fact, after overcoming an energy barrier of 0.46 eV, the water molecule could dissociate into OH and H species [55], the latter configuration being ~ 50% more exothermic than the molecular one.

Table 1

Figure 5

Our calculated adsorption energy values for phenol interactions are listed in Table 2. Considering phenol adsorption, our results indicate that the interactions on the clean structural–oxygen–deficient $Ce_{0.875}Mn_{0.125}O_{1.9375}(111)$ surface is very weak. As can be seen, the phenol molecule preferentially interacted with a Ce cation first neighbor of a Mn dopant (Ce5, $\Delta E_{ads,Phenol}$ = –0.62 eV) (see Fig. 6a). Consequently, the OH group of phenol weakened. The $(O–H)_{phenol}$ distance stretched up to 1.69 Å and H_{phenol} bonded to the nearest surface oxygen forming a $H–O_{surf}$ bond of about 1 Å length. This value is close to that of 0.98 Å, recently reported from DFT calculations in the case of water dissociation on the same surface [68]. The experimental O–H distance in free phenol is 0.958 Å [66], while computational calculations predict a distance in the range [0.940 Å – 0.992 Å], depending on the theory level [69]. These data confirm an elongation of the $(O–H)_{phenol}$ bond. The aromatic ring is bonded to the Ce cation at a bond distance of 2.32 Å (see Fig. 6a). This value is quite similar to the length of Ce–O bonds in pure CeO_2 (2.37 Å). Due to phenol interaction, oxygen anions neighboring the phenol molecule moved ~ 0.1 Å away from the surface, while the O_{surf} bonded to H_{phenol} moved upwards 0.35 Å.

On the other hand, phenol interaction with the hydroxylated H–OH/$Ce_{0.875}Mn_{0.125}O_{1.9375}(111)$ surface is defined by its chemisorptive character. This interaction ($\Delta E_{ads,Phenol}$ = –1.13 eV) was 0.51 eV stronger than that of phenol on the clean surface. Due to phenol chemisorption on the hydroxylated surface, $(O–H)_{phenol}$ stretched up to 1.94 Å (see Fig. 6b) allowing the bonding of a hydrogen (that of the OH_{phenol} group) to a surface oxygen (O_{Mn}). Moreover, the remaining $C_6H_5–O$ fraction was located in a bridge position between Mn and Ce cations with a tilt angle of 69.62º, leading to O_{phenol}–Ce and O_{phenol}–Mn distances of 2.48 Å and 3.75 Å, respectively. This result could be interpreted as an indication of phenolate–type species formation due to phenol strong interactions on the hydroxylated Mn–Ce oxide catalyst surface.

In this regard, we also present a graph of charge distribution for the adsorption zone. Figure 6c, shows the isosurface of charge density difference ($\Delta\rho$), which was obtained as: $\Delta\rho = \rho_{Phenol/Surface} - \rho_{Phenol} - \rho_{Surface}$. In this equation, $\rho_{Phenol/Surface}$ represents the charge density of the system formed by phenol adsorbed on the H–OH/$Ce_{0.875}Mn_{0.125}O_{1.9375}$(111) surface; while $\rho_{Surface}$ and ρ_{Phenol} indicate the charge density of the hydroxylated surface and the phenol molecule, respectively. As it can be seen in Fig. 6c, there is an increase of electron density between phenolate species and surface hydroxyls and Ce and Mn cations. In addition to the charge density rearrangement, there were also significant relaxations of surface ions. The Ce4 and Ce6 cations moved 0.17 Å out from the surface, while the involved Mn dopant displaced not only 0.71 Å on the (111) plane but also 0.11 Å out from the surface. At the same time, several surface and subsurface O anions became strongly relaxed, showing displacements in a range between 0.2 Å and 1.2 Å.

Figure 6 (a–c)

In previous work, D´Alessandro et al. demonstrated that phenol adsorption is favored in the presence of Mn–Ce composites [24]. In the present case, the adsorption of phenol on $Ce_{0.90}Mn_{0.10}O_x$ has been investigated using DRIFT spectroscopy (see Fig. 7). DRIFT spectra show four bands between 1650 and 1200 cm^{-1}. D´Alessandro et al. indicated that these bands can be assigned to the presence of aromatic groups and phenoxy species [70]. In addition, Fig. 7 shows different bands between 1200 and 1000 cm^{-1}. The bands at 1210, 1171 and 1064 cm^{-1} are attributed to C–O vibrations, OH deformation of phenol, and the formation of adsorbed phenolate, respectively.

Figure 7

According to Mathew et al. [71], the band at 1210 cm^{-1} is a consequence of the loss of H (which belongs to OH_{phenol}) and the formation of a phenoxy group on the surface. These authors have shown that the presence of this band at 1210 cm^{-1} and the absence of bands between 2100 and 1700 cm^{-1} are experimental evidence that phenol is not adsorbed perpendicular to the surface. As mentioned before, the tilted configuration and formation of a phenoxy group differ from the reported geometries for phenol adsorption on transition metal surfaces, where the phenyl ring plays a major role in the bonding [35,36]. Therefore, taking into account our theoretical and experimental results it can be assumed that first steps of phenol molecule interactions

on low doping Mn–Ce composite oxide involve its adsorption as a phenoxy group with a tilt angle of about 70° with respect to the hydroxylated surface.

5. Conclusions

$Ce_{0.9}Mn_{0.1}O_x$ solid was synthesized by a coprecipitation method, characterized by XRD and TPR, and evaluated for phenol adsorption. The characterization results showed the formation of CeO_2 and the partial replacement of Ce^{4+} by Mn. TPR results demonstrated that reducibility of Mn and oxygen mobility improved. The theoretical results showed that the water molecule is adsorbed on a Mn cation and the phenol molecule interacts with a Ce cation first neighbor of the Mn dopant. Besides, the adsorbed water became dissociated on the Mn cation, promoting phenol dehydrogenation. Therefore, the phenol molecule chemisorbed as a phenoxy–type species with a titled angle of ca. 70º, in agreement with DRIFTS results.

In summary, our theoretical and experimental results indicated the formation of a solid solution where the Mn dopant replaces the Ce cation. Furthermore, the study showed that the chemisorption of phenol involved the formation of a phenoxy group, linked to the surface, with the aromatic ring tilted to the surface.

Acknowledgements

The authors thankfully acknowledge financial support from the Universidad de Buenos Aires (UBACyT–20020110200044), SGCyT–Universidad Nacional del Sur, Universidad Nacional de La Plata, CONICET (PIP 942 and 2014–2016), ANPCyT (PICT 2011–1312 and 2014–1351) and CIC–Pcia. de Buenos Aires. A. Juan and J. Sambeth are members of CONICET.

References

[1] A.Trovarelli, Catalysis by Ceria and Related Materials, Imperial College Press, London, 2002.

[2] J. Paier, Ch. Penschke, J. Sauer, Oxygen defects and surface chemistry of ceria: Quantum chemical studies compared to experiment, Chem. Rev. 113 (6) (2013) 3949–3985.

[3] E. Aneggi, M. Boaro, C. Leitenburg, G. Dolcetti, A. Trovarelli, Insights into the redox properties of ceria–based oxides and their implications in catalysis, J. Alloys Comp. 408 (2006) 1096–1102.

[4] J. Kašpar, P. Fornasiero, M. Graziani, Use of CeO_2–based oxides in the three–way catalysis, Catal. Today 50 (1999) 285–298.

[5] C. Zhang, A. Michaelides, D. King, S. Jenkins, Oxygen vacancy clusters on ceria: Decisive role of cerium f electrons, Phys. Rev. B 79 (2009) 075433(1–11).

[6] P. Dholabhai, J. Adams, P. Crozier, R. Sharma, Oxygen vacancy migration in ceria and Pr–doped ceria: A DFT+U study, J. Chem. Phys. 132 (2010) 094104(1–8).

[7] Z. Yang, Y. Wei, Z. Fu, K. Hermansson, Facilitated vacancy formation at Zr–doped ceria(1 1 1) surfaces, Surf. Sci. 602 (2008) 1199–1206.

[8] Q. Liang, X. Wu, D. Weng, H. Xu, Oxygen activation on Cu/Mn–Ce mixed oxides and the role in diesel soot oxidation, Catal. Today, 139 (2008) 113–118.

[9] H. Chen, A. Sayari, A. Adnot, F. Larachi, Composition–activity effects of Mn–Ce–O composites on phenol catalytic wet oxidation, Appl. Catal. B: Environ. 32 (2001) 195–204.

[10] M. Zhang, D. Jiang, H. Jiang, Enhanced oxygen storage capacity of $Ce_{0.88}Mn_{0.12}O_y$ compared to CeO_2: An experimental and theoretical investigation, Mater. Res. Bull. 47 (2012) 4006–4012.

[11] W. Hong, S. Iwamoto, S. Hosokawa, K. Wada, H. Kanai, M. Inoue, Effect of Mn content on physical properties of CeO_x–MnO_y support and BaO–CeO_x–MnO_y catalysts for direct NO decomposition, J. Catal. 277 (2011) 208–216.

[12] D. Delimaris, T. Ioannides, VOC oxidation over MnO_x–CeO_2 catalysts prepared by a combustion method, Appl. Catal. B: Environ. 84 (2008) 303–312.

[13] W. Shan, N. Ma, J. Yang, X. Dong, C. Liu, L. Wei, Catalytic oxidation of soot particulates over MnO_x–CeO_2 oxides prepared by complexation–combustion method, J. Nat. Gas Chem. 19 (2010) 86–90.

[14] M. Abecassis–Wolfovich, R. Jothiramalingam, M. Landau, M. Herskowitz, B. Viswanathan, T. Varadarajan, Cerium incorporated ordered manganese oxide OMS–2 materials: Improved catalysts for wet oxidation of phenol compounds, Appl. Catal. B: Environ. 59 (2005) 91–98.

[15] L. Shi, W. Chu, F. Qu, S. Luo, Low–temperature catalytic combustion of methane over MnO_x–CeO_2 mixed oxide catalysts: Effect of preparation method, Catal. Lett. 113 (1) (2007) 59–64.

[16] X. Tang, Y. Li, X. Huang, Y. Xu, H. Zhu, J. Wang, W. Shen, MnO_x–CeO_2 mixed oxide catalysts for complete oxidation of formaldehyde: Effect of preparation method and calcination temperature, Appl. Catal. B: Environ. 62 (2006) 265–273.

[17] G. Zhou, P. Shah, R. Gorte, A study of cerium–manganese mixed oxides for oxidation catalysis, Catal. Lett. 120 (3) (2008) 191–197.

[18] Y. Tu, M. Meng, Zh. Sun, L. Zhang, T. Ding, T. Zhang, CO preferential oxidation over Au/MnO_x–CeO_2 catalysts prepared with ultrasonic assistance: Effect of calcination temperature, Fuel Process. Technol. 93 (2012) 78–84.

[19] Q. Guo, Y. Liu, MnO_x modified Co_3O_4–CeO_2 catalysts for the preferential oxidation of CO in H_2–rich gases, Appl. Catal. B: Environ. 82 (2008) 19–26.

[20] D. Duprez, F. Delanoe, J. Barbier, P. Isnard, G. Blanchard, Catalytic Oxidation of Organic Compounds in Aqueous Media, Catal. Today 29 (1996) 317–322.

[21] L. Yang, Z. Chen, D. Zhang, Y. Liu, Y. Han, J. Shen, Adsorption of dimethylamine from aqueous solution by manganese dioxide. Water Sci Technol. 63(1) (2011) 45–50.

[22] B. Hu, Ch. Chen, S. Frueh, L. Jin, R. Joesten, S. Suib, Removal of aqueous phenol by adsorption and oxidation with doped hydrophobic cryptomelane–type manganese oxide (K−OMS–2) nanofibers. J. Phys. Chem. C 114(21) (2010) 9835–9844.

[23] K. Parida, A. C. Pradhan, Removal of phenolic compounds from aqueous solutions by adsorption onto manganese nodule leached residue, J. Hazard. Mater., 173(1–3) (2010) 758–764.

[24] O. D´Alessandro, H. Thomas, J. Sambeth, An analysis of the first steps of phenol adsorption–oxidation over coprecipitated Mn–Ce catalysts: a DRIFTS study, Reac. Kinet. Mech. Catal. 107 (2) (2012) 295–309.

[25] S. Hamoudi, F. Larachi, A. Sayari, Wet oxidation of phenolic solutions over heterogeneous catalysts–degradation profile and catalyst behavior, J. Catal. 177 (1998) 247–258.

[26] M. Abecassis–Wolfovich, M.V. Landau, A. Brenner, M. Herskowitz, Catalytic wet oxidation of phenol with Mn−Ce–based oxide catalysts: impact of reactive adsorption on TOC removal, Ind. Chem. Eng. Res. 43 (2004) 5089–5097.

[27] M. Abecassis–Wolfovich, R. Jothiramalingam, M.V. Landau, M. Herskowitz, B. Viswanathan, T. Varadarajan. Cerium incorporated ordered manganese oxide OMS–2 materials: Improved catalysts for wet oxidation of phenol compounds. Appl. Catal. B: Environ. 59 (1–2) (2005) 91–98.

[28] F. Arena, J. Negro, A. Parmaliana, L. Spadaro, G. Trunfio, Improved MnCeOx systems for the catalytic wet oxidation (CWO) of phenol in wastewater streams. Ind. Eng. Chem. Res. 46(21) (2007) 6724– 6731.

[29] L. D. Site, A. Alavi, C. F. Abrams, Adsorption energies and geometries of phenol on the (111) surface of nickel: An ab initio study, Phys. Rev. B – Cond. Matter & Mater. Phys. 67 (19) (2003) 193406.

[30] L. M. Ghiringhelli, R. Caputo, L. D. Site, Phenol near Ni(111), Ni(110), and Ni(221) surfaces in a vertical ring geometry: A density functional study of the oxygen–surface bonding and O–H cleavage Phys. Rev. B – Cond. Matter & Mater. Phys. 75 (11) (2007) 113403.

[31] M. Altarawneh, M. W. Radny, P. V. Smith, J. C. Mackie, E. M. Kennedy, B. Z. Dlugogorski, 2–Chlorophenol adsorption on Cu(1 0 0): First–principles density functional study Surf. Sci., 602 (8) (2008) 1554–1562.

[32] M. Altarawneh, M. W. Radny, P. V. Smith, J. C. Mackie, E. M. Kennedy, B. Z. Dlugogorski, Adsorption of chlorophenol on the Cu(1 1 1) surface: A first–principles density functional theory study, App. Surf. Sci., 254 (14) (2008) 4218–4224.

[33] N. Jayanthi, J. Cruz, T. Pandiyan, DFT studies on the phenol and thiophenol interaction on an undecagold cluster surface, Chem. Phys. Lett., 455 (1–3) (2008) 64–71.

[34] A.J.R Hensley, Y. Wang, J.–S. McEwen, Adsorption of phenol on Fe (110) and Pd (111) from first principles, Surf. Sci. 630 (2014) 244–253.

[35] A.J.R Hensley, Y. Wang, J.–S. McEwen Phenol deoxygenation mechanisms on Fe(110) and Pd(111) ACS Catal. 5(2) (2015) 523–536.

[36] G. Li, J. Han, H. Wang, X. Zhu, Q. Ge, Role of dissociation of phenol in its selective hydrogenation on Pt(111) and Pd(111), ACS Catal. 5 (3) (2015) 2009–2016.

[37] J. Zhao, B. Gao, Q. Cai, X. Wang, X. Wang, Theoretical study of phenol adsorption on the (8, 0) silicon carbide nanotube Theor. Chem. Acc., 129(1) (2011) 85–92.

[38] A.A. Peyghan, M.T. Baei, M. Moghimi, S. Hashemian, Phenol adsorption study on pristine, Ga–, and In–doped (4,4) armchair single–walled boron nitride nanotubes Comp. & Theor. Chem. 997 (2012) 63–69.

[39] A.A. Peyghan, M.T. Baei, M. Moghimi, S. Hashemian, Theoretical Study of Phenol Adsorption on Pristine, Ga–Doped, and Pd–Decorated (6,0) Zigzag Single–Walled Boron Phosphide Nanotubes, J. Clust. Sci. 24 (1) (2013) 49–60.

[40] A. Soltani, M. T. Baei, M. R. Taghartapeh, E. T. Lemeski, S. Shojaee, Phenol interaction with different nano–cages with and without an electric field: a DFT study Struct. Chem. (2014) 9 p. Article in Press.

[41] J.M. Galicia Hernández, G. H. Cocoletzi, E. C. Anota, DFT studies of the phenol adsorption on boron nitride sheets, J. Mol. Model. 18 (1) (2012) 137–144.

[42] J. M. Galicia Hernández, E. C. Anota, M. T. Romero De La Cruz, M. G. Melchor, G. H. Cocoletzi, First principles studies of the graphene–phenol interactions, J. Mol. Model. 18 (8) (2012) 3857–3866.

[43] L. M. Cam, L.Van Khu, N. N. Ha, Theoretical study on the adsorption of phenol on activated carbon using density functional theory J. Mol. Model. 19 (10), (2013) 4395–4402.

[44] B. Shong, S. F. Bent, Transition in the molecular orientation of phenol adsorbates on the Ge(100)–2 × 1 surface, J. Phys. Chem. C, 116 (14) (2012) 7925–7930.

[45] M. Carbone, S. Meloni, R. Caminiti, Dissociative versus molecular adsorption of phenol on Si (100) 2×1: A first–principles calculation, Phys. Rev. B – Cond. Matter & Mater. Phys. 76 (8) (2007) 085332.

[46] M. Carbone, P. Cazzato, R. Caminiti, Coverage effects on phenol adsorption on Si(1 0 0)2 × 1 as: A first principle calculation, Surf. Sci. 603 (4) (2009) 611–619.

[47] S. D. Chakarova–Käck, Ø.Borck, E. Schröder, B. I. Lundqvist, Adsorption of phenol on graphite(0001) and α– Al_2O_3 (0001): Nature of van der Waals bonds from first–principles calculations, Phys. Rev. B – Cond. Matter & Mater. Phys. 74 (15) (2006) 155402.

[48] J. Blomqvist, P. Salo, Adsorption of benzene, phenol, propane and carbonic acid molecules on oxidized Al(111): A first–principles study, J. Phys. Cond. Matter, 21 (22) (2009) 225001.

[49] M. Altarawneh, M. W. Radny, P. V. Smith, J. C. MacKie, E. M. Kennedy, B. Z. Dlugogorski, A. Soon, C. Stampfl, A first–principles density functional study of chlorophenol adsorption on Cu_2O(110):CuO J. Chem. Phys. 130 (18) (2009) 184505.

[50] Y. Tang, H. Zhang, L. Cui, C. Ouyang, S. Shi, W. Tang, H. Li, J. Lee, L. Chen, First–principles Investigation on Redox Properties of M–doped CeO_2 (M=Mn,Pr,Sn,Zr), Phys. Rev. B 82 (2010) 125104.

[51] A. Gupta, U. V. Waghmare, M. S. Hegde, Correlation of Oxygen Storage Capacity and Structural Distortion in Transition–metal–, Noble–metal–, and Rare–earth–ion–Substituted CeO_2 from First Principles Calculation, Chem. Mater. 22 (2010) 5184–5198.

[52] W. Cen, Y. Liu, Z. Wu, H. Wang, X. Weng, A Theoretic Insight Into The Catalytic Activity Promotion of CeO_2 Surfaces by Mn Doping, Phys. Chem. Chem. Phys. 14 (2012) 5769–5777.

[53] M. Zhang, D. Jiang, H. Jian, Enhanced Oxygen Storage Capacity of $Ce_{0.88}Mn_{0.12}O_y$ Compared to CeO_2: An Experimental and Theoretical Investigation, Mater. Res. Bull. 47 (2012) 4006–4012.

[54] S. Imamura, Y. Uematsu, K. Utani, T. Ito, Combustion of formaldehyde on ruthenium/cerium(IV) oxide catalyst, Ind. Eng. Chem. Res. 30 (1) (1991) 18–21.

[55] D. García Pintos, A. Juan, B. Irigoyen, Mn–Doped CeO_2: DFT+U Study of a Catalyst for Oxidation Reactions, J. Phys. Chem. C 117 (35) (2013) 18063– 18073.

[56] L. Qu, C. Li, C. Zeng, M. Zhang, M. Fu, J. Ma, F. Zhan, D. Luo, Support modification for improving the performance of MnOx–CeOy/γ–Al_2O_3 in selective catalytic reduction of NO by NH_3, Chem. Eng. J. 242 (2014) 76–85.

[57] J. Traawczynski, B. Bielak, W. Mista, Oxidation of ethanol over supported manganese catalysts—effect of the carrier, Appl. Catal. B 55 (4) (2005) 277–285.

[58] F. Kapteijn, L. Singoredjo, A. Andreini, Activity and selectivity of pure manganese oxides in the selective catalytic reduction of nitric oxide with ammonia. Appl. Catal. B 3 (2–3) (1994) 173–189.

[59] G. Qi, R. Yang, R. Chang, MnOx–CeO_2 mixed oxides prepared by co–precipitation for selective catalytic reduction of NO with NH_3 at low temperatures, Appl. Catal. B, 51(2) (2004) 93–106.

[60] D. García Pintos, A. Juan, B. Irigoyen, Density functional theory study of water interactions on Mn–doped CeO_2(111) surface, Appl. Surf. Sci. 313 (2014) 784–793.

[61] G. Kresse, J. Furthmuller, Efficiency of ab–initio total energy calculations for metals and semiconductors using a plane–wave basis set, Comp. Mater. Sci. 6(1) (1996) 15–50.

[62] G. Kresse, J. Hafner, Ab initio molecular dynamics for liquid metals. Phys. Rev. B 47(1) (1993) 558–561.

[63] J. Perdew, K. Burke, M. Ernzerhof, Generalized Gradient Approximation Made Simple, Phys. Rev. Lett. 77(18) (1996) 3865–3868.

[64] G. Kresse, D. Joubert, From ultrasoft pseudopotentials to the projector augmented–wave method, Phys. Rev. B 59(3) (1999) 1758–1775.

[65] H. Monkhorst, T. Pack, Special points for Brillouin–zone integrations, Phys. Rev. B. 13(12) (1976) 5188–5192.

[66] S. Dudarev, G. Botton, S. Savrasov, C. Humphreys, A. Sutton, Electron–energy–loss spectra and the structural stability of nickel oxide: An LSDA+U study, Phys. Rev. B 57(3) (1998) 1505–1509.

[67] V. Anisimov, J. Zaanen, O. Andersen, Band theory and Mott insulators: Hubbard U instead of Stoner I, Phys. Rev. B 44 (3) (1991) 943–954.

[68] H. Lampert, W. Mikenda, A. Karpfen, Molecular Geometries and Vibrational Spectra of Phenol, Benzaldehyde, and Salicylaldehyde: Experimental versus Quantum Chemical Data, J. Phys. Chem. A 101 (1997) 2254–2263.

[69] K. Gross, P. G. Seybold, Substituent Effects on the Physical Properties and pKa of Phenol, Inter. J. Quant Chem. 85 (2001) 569–579.

[70] O. D´Alessandro, H. Thomas, J. Sambeth, Synthesis, Characterization and Study of Phenol Adsorption Over MnO_x–CeO_2, Curr. Catal. 3 (2) (2014) 166–171.

[71] Th. Matthew, M. Vijayaraj, Sh. Pai, B. Tope, S. Hedge, S. Rãs, Ch. Gopinath, A mechanistic approach to phenol methylation on $Cu_{1-x}Co_xFe_2O_4$: FTIR study, J. Catal. 227(1) (2004) 175–185.

CAPTIONS FOR FIGURES

Figure 1. X–ray diffraction (XRD) spectra of $Ce_{0.90}Mn_{0.10}O_x$ and CeO_2 samples.

Figure 2. Ce–Mn–O bulk supercell with oxygen vacancies.

Figure 3. H_2–TPR profiles of MnO_x and $Ce_{0.90}Mn_{0.10}O_x$ samples.

Figure 4 The structural–oxygen–deficient $Ce_{0.875}Mn_{0.125}O_{1.9375}$(111) model surface. (a) slab side view. (b) Top view. Different Ce cations and O anions were labeled.

Figure 5. Water dissociative adsorption on the structural–oxygen–deficient $Ce_{0.875}Mn_{0.125}O_{1.9375}$(111) model surface.

Figure 6. Preferential phenol interactions on the $Ce_{0.875}Mn_{0.125}O_{1.9375}$(111) model surface. (a) Phenol interaction on the bare surface. (b) Phenol chemisorption on the hydroxylated surface. (c) Isosurface of charge density difference for the adsorption zone corresponding to phenol interaction on the hydroxylated surface.

Figure 7. DRIFTS spectra of phenol adsorption on $Ce_{0.90}Mn_{0.10}O_x$ solid sample.

Table 1. Calculated H_2O adsorption energy values for both the molecular and the dissociated interactions on the structural-oxygen–deficient $Ce_{0.875}Mn_{0.125}O_{1.9375}$(111) model surface.

Cation site*	Molecular interactions, $\Delta E_{ads,H2O}$ (eV)	Dissociated interactions, $\Delta E_{ads,H–OH}$ (eV)
Mn	–0.81	–1.22
Ce6	–0.53	–0.34
Ce5	–0.50	–0.51
Ce2	–0.44	–0.68
Ce7	–0.29	–0.28

* The cation labels are the same as those indicated in Fig. 4b.

Table 2. Calculated adsorption energy values for phenol interactions on the bare and hydroxylated $Ce_{0.875}Mn_{0.125}O_{1.9375}(111)$ model surfaces.

Model Surface	Site*	Phenol interactions, $\Delta E_{ads,Phenol}$ (eV)
$Ce_{0.875}Mn_{0.125}O_{1.9375}(111)$	Mn	–0.22
	Ce6	–0.46
	Ce5	–0.62
	Ce2	–0.33
	Ce7	–0.36
$H–OH/Ce_{0.875}Mn_{0.125}O_{1.9375}(111)$	Bridge Mn–Ce2	–1.13

* The cation labels are the same as those indicated in Fig. 4b.

Highlight

1.- Phenol is adsorbed on the structural–oxygen–deficient Ce-Mn-O (111) surface interacting with the Ce cation first neighbor to Mn dopant.

2- The O-H of the phenol group bond is stretched up to 1.69 Å.

3- Phenol interaction with the hydroxylated $H–OH/Ce_{0.875}Mn_{0.125}O_{1.9375}(111)$ surface is 0.51 eV stronger than on the clean surface.

4. The $C_6H_5–O$ fraction is adsorbed in a bridge position between Mn and Ce cations with a tilt angle of 69.62º in agreement with IR data